Time reversal in a waveguide: Study of the temporal and spatial focusing

Philippe Roux[a] and Mathias Fink
Laboratoire Ondes et Acoustique, ESPCI, Université Paris VII, CNRS UMR 7587, 10 rue Vauquelin, 75005 Paris, France

(Received 24 February 1999; accepted for publication 17 February 2000)

Temporal and spatial focusing properties of time-reversal mirrors (TRMs) are studied in a waveguide. The experiments are done using an ultrasonic TRM in an idealized waveguide. The width of the focal spot, and the spatial and temporal sidelobe levels are experimentally and numerically analyzed with respect to the characteristics of the waveguide-TRM system. An algorithm is developed to compute directly in the time domain the time-reversed field. This algorithm is based on the application of the mirror theorem to both the source and the TRM placed in the waveguide. Because time reversal is a stable and robust process, some of the ultrasonic results can be extended to ocean acoustics. Applications to underwater acoustic transmissions as well as ultrasonic medical imaging are discussed. © *2000 Acoustical Society of America.* [S0001-4966(00)04205-3]

PACS numbers: 43.30.Pc, 43.20.Gp, 43.35.Cg [DLB]

INTRODUCTION

Time-reversal invariance in acoustics means that for every burst of sound emitted from a source—and possibly reflected, refracted, or scattered by any propagation medium—there exists a set of waves that precisely retraces all these complex paths and converges at the original source, as if time were going backwards. Based on this concept, time-reversal cavities[1,2] and time-reversal mirrors (TRMs)[3–6] have been developed to focus ultrasonic pulses through strongly heterogeneous media such as multiscattering media,[7] chaotic cavities,[8] or waveguides.[9] The advantage of time reversal, compared to any other technique, is that it provides a robust set of waves without any signal analysis, which compensates for the transfer function of the medium. Thus, TRMs lead to a spatial focusing and a temporal compression. Spatial focusing means that the time-reversed field focuses back exactly at the source. Temporal compression means that the time-reversed signal at the source is similar to the signal previously emitted by the source. Recently, we have shown that a TRM takes advantage of the heterogeneity of the medium to improve the focusing quality at the source.[7] Following these results, the aim of this paper is twofold: on the one hand, we carefully study the spatial and temporal focusing properties of an ultrasonic TRM in a waveguide; on the other hand, we show that some of these results may be extended in ocean acoustics with some applications to acoustic transmission in an underwater acoustic channel. However, time reversal in underwater acoustics is not a new field. In the sixties, Parvulescu *et al.*[10,11] performed experiments in shallow water at sea with one transducer working in a time-reversed mode. They observed temporal compression and they explained the major results by the method of images we will use in Sec. I. Nevertheless, their experiments did not embody the spatial focusing property of TRMs. More recently, Jackson *et al.*[12,13] and Dowling[14,15] have developed the theory of phase conjugation (the Fourier conjugate of time reversal) in ocean acoustics. At the same time, Feuillade *et al.*[16] computed numerical time-reversal experiments in shallow water where spatial focusing was studied. Finally, Kuperman *et al.*[17] and Hodgkiss *et al.*[18] demonstrated time-reversal experiments in an underwater acoustic channel. At a 445-Hz frequency, they used a 24-elements TRM to perform focusing and multipaths compensation up to 30 km. One of their important results was to show that time reversal is a very robust and stable process which is not very sensitive to noise or ocean variability. Thus, when performing a time-reversal experiment, the focusing in a ''real'' environment (the ocean) and an idealized system (an ultrasonic waveguide) are quite comparable. Working with ultrasound may then be a good way, particularly cheap and easy to set up, to study time-reversal properties in a waveguide very generally.

The paper is structured as follows: In Sec. I, we describe the experimental setup and the basic results obtained after time reversal in a waveguide. In Sec. II, we represent the TRM-waveguide system with its analog in free space and we deduce from this representation a simple way to compute, directly in the time domain, the acoustic focusing after time reversal. In Sec. III, we experimentally and numerically study the focal spot and the sidelobe levels as a function of the characteristics of the system: the length (L) and the height (H) of the guide, the wavelength (λ), and the number of transducers (N) of the TRM. In Sec. IV, we study the temporal compression after time reversal as a function of the same parameters. These results lead to the application of time reversal to acoustic transmission in an underwater acoustic channel as well as to medical applications in ultrasonics. Finally, we present our investigations of the influence of a nonstatic interface (such as waves at the surface of the ocean) on the quality of the time-reversal focusing.

[a]Electronic mail: Philippe.Roux@espci.fr

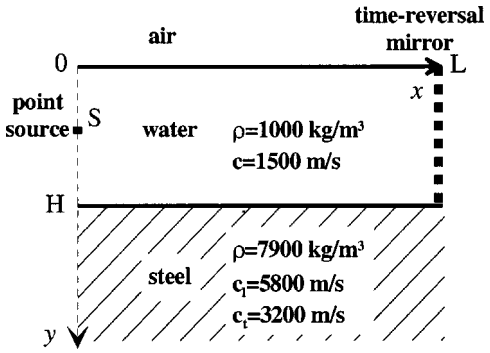

FIG. 1. Schematic of the acoustic waveguide: the guide length (L) ranges from 40 to 80 cm and the water depth (H) from 1 to 5 cm. The central acoustic wavelength (λ) is 0.5 mm. The array element spacing is 0.42 mm. The TRM is always centered at the middle of the water depth.

I. EXPERIMENTAL SETUP AND FIRST RESULTS

In this section, we describe first the basics of a time-reversal experiment and we show that the time-reversal focusing properties are greatly improved when the TRM is placed in a confined medium.

The setup for a time-reversal experiment in a waveguide is presented in Fig. 1. The water channel is bounded by two interfaces. A point-like ultrasonic source is located on one side of the waveguide and can be used either as a source or as a receiver. A time-reversal mirror is located at a distance L from the source. A complete time-reversal experiment is divided in three stages: first, the transducer source located at S transmits a pulse. In the second stage, the incident field is recorded, time-reversed, and transmitted back into the waveguide. In the last stage, the time-reversed field is measured in the source plane by the source transducer, which is used as a receiver. This mobile receiver can be translated around the initial position S along the y axis to measure step by step the time-reversed pressure field $p_{\mathrm{tr}}(y,t)$. In this case we are interested both in the temporal compression and in the spatial focusing of the time-reversed field in the plane of the initial source. The quality of the temporal compression at the source can be deduced from the curve $p_{\mathrm{tr}}(0,t)$ and the directivity pattern of the time-reversed beam is obtained from the curve $d(y)=\max_t\{p_{\mathrm{tr}}(y,t)\}$.

The waveguide is made of two plane-parallel interfaces (one steel/water and one air/water interface). The length of the guide ranges from $L=400$ mm to $L=800$ mm, and the water depth from $H=10$ mm to $H=50$ mm. The TRM is a 128-transducer linear array identical to the source transducer. The width of an individual element is 0.39 mm, and the spacing between two elements is 0.42 mm. Thus, the maximal aperture of the array is 50 mm. The number of elements used during a time-reversal experiment is then adjusted to the water depth (for example, only 96 transducers are used for a 4-cm-depth waveguide). The mirror works at a 3-MHz central frequency with a 50% relative bandwidth at -6 dB (central wavelength$=0.5$ mm). Each transducer element has its own amplifier, an 8-bit A/D converter, a storage memory, and an 8-bit D/A converter working at a 20-MHz sampling rate, which permit us to retransmit a time-reversed version of the recorded signals.

Several comments are to be made about the experimental setup:

(i) The length of the source and the length of the array elements are $d=12$ mm, which is significantly larger than the wavelength and the width of each element. However, these transducers cannot be considered as line sources because the propagation distance L is always much larger than the far-field distance R_{farfield} of each of them ($R_{\mathrm{farfield}}\approx d^2/4\lambda=72$ mm). Thus, the source and the TRM lie in each other's far field and the acoustic radiation is inversely proportional to the range, as for a point-like source.

(ii) The steel density is 7.9 and the longitudinal and transversal wave speeds are $c_1=5800$ m/s and $c_t=3200$ m/s, respectively. With these parameters, no energy penetrates into the bottom for grazing angles smaller than $\theta_c=65°$ (grazing angles are measured with respect to a horizontal axis). This critical angle is much larger than the angular directivity of our ultrasonic transducers, which means that no energy is dissipated into the bottom.

(iii) The TRM is always centered at the middle of the water depth, whatever the number of transducers used. However, the source transducer will not always be placed at the center of the waveguide.

(iv) The sidewalls of the tank are at more than 30 cm from the xy propagation plane. Given the waveguide length, this means that the first echoes from the tank boundaries, if any, would arrive much later than the last recorded echoes reflected by the waveguide interfaces [see Fig. 2(a)].

Figure 2(a) shows the transmitted field recorded by the array after propagation through the waveguide. After arrival of a first wavefront corresponding to the direct path, we notice the arrival of a set of multipath signals corresponding to the multiple reflections of the incident wave on the interfaces. Figure 2(b) represents the signal recorded on one transducer of the TRM. After time reversal, Fig. 3(a) shows a remarkable temporal and spatial focusing of the time-reversed field at the initial source. Two major points are to be underlined: from the temporal point of view, multipath effects are compensated. The signal measured at S in the waveguide is nearly identical to the one you would find after a time-reversal experiment in free space [Fig. 3(b)]. This means that the transfer function of the waveguide has been completely compensated by the time-reversal process. Second, from the spatial point of view, the time-reversal focusing is much smaller than the one observed after a time-reversal experiment with the same TRM in free space (Fig. 4). Thus, time reversal takes advantage of the presence of interfaces in the medium to improve spatial focusing.

Following these first results, we study now the temporal and spatial properties of time-reversal focusing in a waveguide and some of its applications in ultrasonics and ocean acoustics.

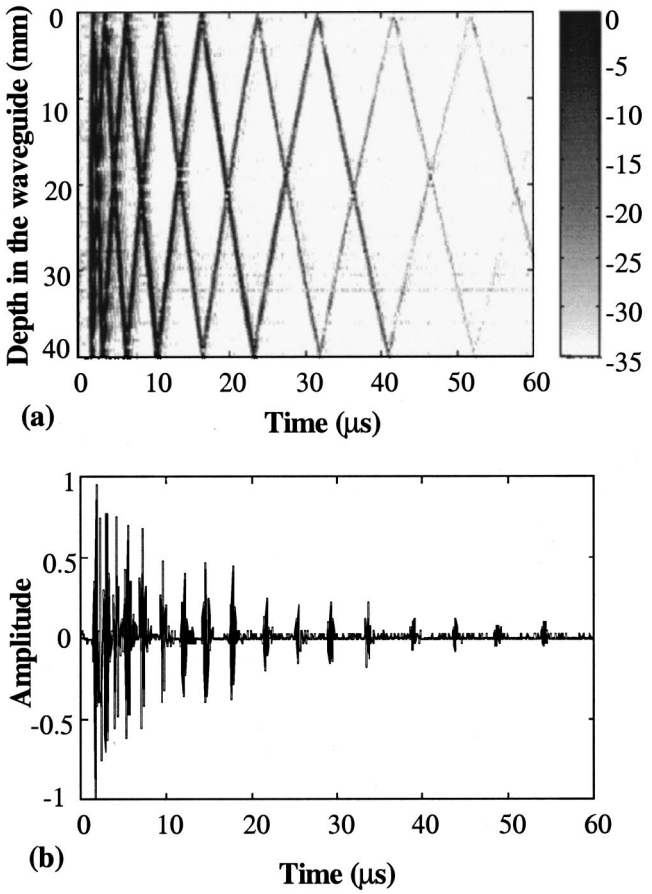

FIG. 2. (a) Spatial-temporal representation of the incident acoustic field received by the TRM after propagation through the guide; $H=40$ mm; $L=74$ cm; source depth=20 mm; (b) Temporal signal measured on one transducer of the array; receiver depth=10 mm.

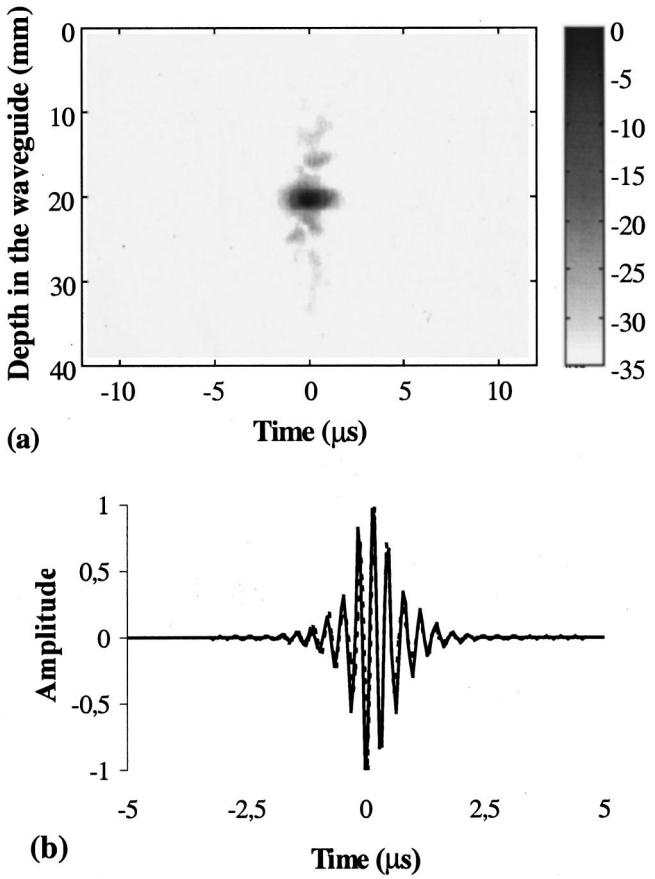

FIG. 3. (a) Spatial-temporal representation of the time-reversed field measured in the plane of the point source; $L=74$ cm; $H=40$ mm; source depth=20 mm; a 96-transducer TRM; (b) bold line: zoom of the time-reversed signal measured at the point source between -5 and $+5$ μs (receiver depth=20 mm); dashed line: time-reversed signal measured at the source in free space.

II. FREE-SPACE REPRESENTATION OF TIME REVERSAL IN A WAVEGUIDE

The goal of this section is to give a free-space representation of the TRM-waveguide system and to deduce from this representation an algorithm to compute directly in the time domain the time-reversed field at the source.

We restrict our work to the study of a Pekeris waveguide.[19] In the experimental configuration, λ is always much smaller than the characteristic lengths of the waveguide L and H. Ray theory can thus be applied to describe acoustic propagation. In this case, Snell's laws imply that each waveguide interface acts as a mirror for acoustic rays. The application of the method of images[20] allows us to transpose the forward and backward propagation in a waveguide between a point source in A and a TRM in B into a free-space configuration. To understand this transposition, we describe time reversal as a two-stage process: the forward and backward propagation.

In a first stage, the signal is emitted from A and is received on the TRM in B after propagation through the waveguide. The rays then appear to be emitted from a set of virtual sources in free space. These sources are the images of the actual source with respect to the guide interfaces (Fig. 5). The signal received on each individual transducer of the TRM is the superposition of the signal coming from each image of the point source A. We experimentally confirm this result by recording the field on the TRM after propagation through the waveguide and by time-reversing this field in free space, meaning we remove the waveguide and transmit the time-reversed signal in a medium without interface. The time-reversed field then focuses at the source but also on the virtual images of the source with respect to the interfaces (Fig. 6). The directivity pattern is asymmetric because the

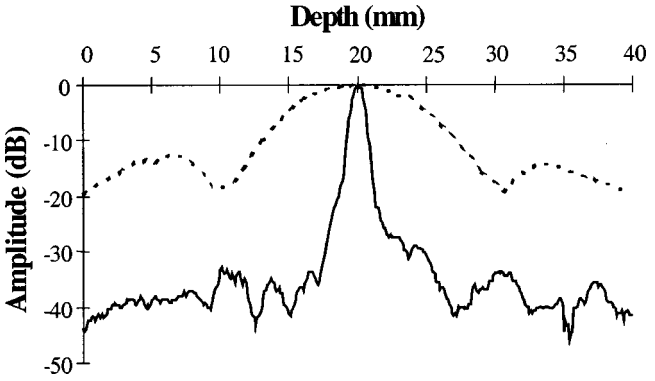

FIG. 4. Directivity pattern of the time-reversed field in the plane of source: the dotted line corresponds to free space, the full line to the waveguide; $H=40$ mm; $L=74$ cm; a 96-transducer TRM; source depth=20 mm.

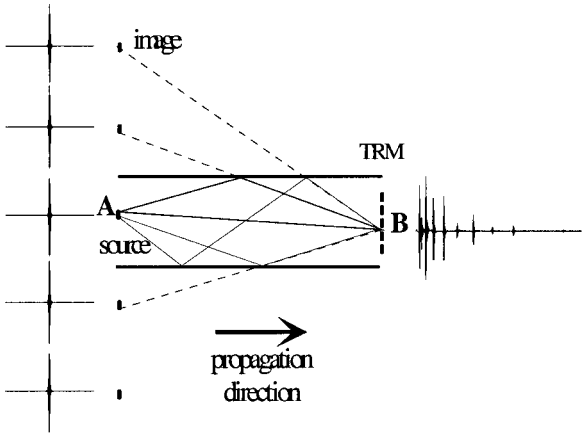

FIG. 5. Application of the method of images to the point source in the waveguide.

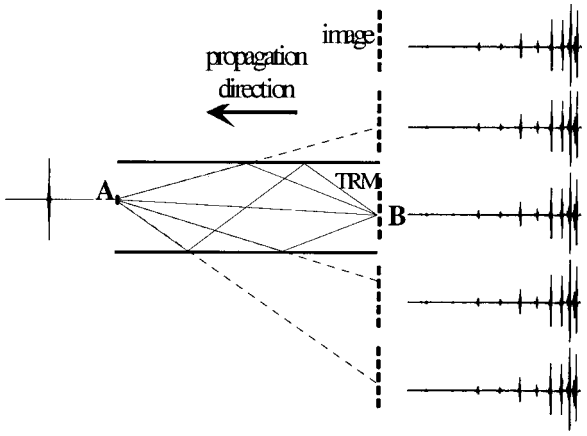

FIG. 7. Application of the method of images to the TRM in the waveguide.

source is not centered at the middle of the water depth: for a source at depth y_0, the images are located at $\pm y_0 \pm 2kH$, where k is an integer.

In a second stage, the time-reversal field is sent back from the TRM in B and we measure in A the time-reversed field after back propagation through the guide. From A, the TRM is now equivalent in free space to a set of virtual TRMs, which are the images of the actual TRM with respect to the wave guide interfaces (Fig. 7). This result has already been shown by the fact that the focal spot after time reversal in the waveguide is much smaller than the one obtained with the same TRM in free space (see Fig. 4). In other words, the smaller focal spot is due to an increase of the effective TRM aperture due to the presence of virtual TRM images in the waveguide.

Thus, the application of the method of images is twofold; it increases the effective number of sources in the forward propagation stage and also the number of TRMs in the backward propagation stage. This allows us to describe the complicated TRM-waveguide system with a simpler free-space system created by a set of sources and mirrors. These sources are the images of the actual source with respect to the interfaces and are placed in front of a set of TRMs, which are the images of the actual TRM with respect to the same interfaces (Fig. 8).

Theoretically the number of images is infinite. However, this number is experimentally limited by two different effects in ocean acoustics and in ultrasonics:

(i) In ocean acoustics, the number of echoes observed in a waveguide is limited by the reflection coefficient at the bottom interface. In first approximation, this leads to an attenuation as a function of range equal to

$$R(\theta_{\text{grazing}}) = R_1^n(\theta_{\text{grazing}}) * (-1)^m, \tag{1}$$

where $R_1(\theta_{\text{grazing}})$ is the reflection coefficient measured at the water–bottom interface for a plane wave and a grazing angle θ_{grazing}, n corresponds to the number of reflections on this interface, and m the number of reflections on the water–air interface. For a given grazing angle θ_{grazing}, the larger the number of reflections (n), the longer the propagation range and the

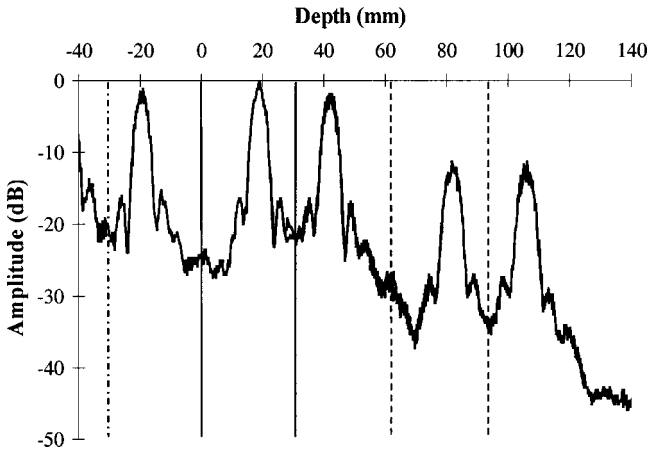

FIG. 6. Directivity pattern of the time-reversed field after back propagation in free space. The bold lines correspond to the waveguide actual interfaces and the dashed lines to the images of the interfaces; $L=33$ cm, $H=32$ mm, a 66-transducer TRM; source depth=19 mm.

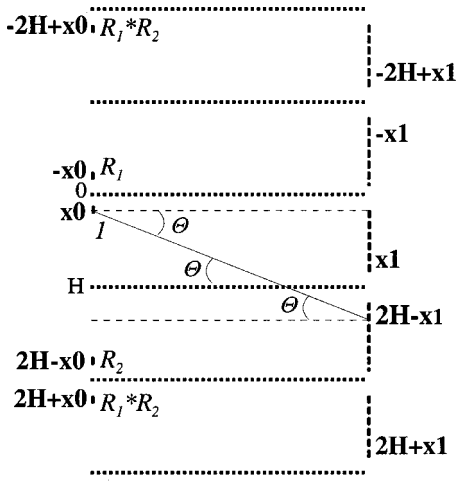

FIG. 8. Representation of the time-reversal–free-space system analog to the time-reversal–waveguide system: on the left are located the images of the actual source x_0 at $\pm x_0 + 2kH$; on the right are located the images of an actual TRM transducer x_1 at $\pm x_1 + 2$ pH. The coefficients $R_1^n * R_2^m$ correspond to the attenuation of every source relative to its position. In the case of a water–air interface, we have $R1 = -1$. A ray is plotted between the source x_0 and the receiver $2H - x_1$. The grazing angle at the interface Θ is equal to the launch and the reception angles.

stronger the attenuation. The reflection coefficient $R1$ may be complex for a reflection below the critical angle θ_c or because of absorption in the bottom.[20] Basically, this reflection coefficient implies that long-distance propagation in ocean waveguides occurs within a cone whose half-angle is equal to the critical angle θ_c.

(ii) In ultrasonics, attenuation due to reflection is negligible in the case of a steel–water interface. However, the size of each transducer is no longer small compared to the acoustic wavelength. This leads to an angular directivity ang(θ_{dir}) which affects the acoustic field both in transmission and in reception. For a launch or a reception angle θ_{dir} (with respect to the horizontal axis), the angular directivity is approximated by an attenuation coefficient equal in the far field to

$$\text{ang}(\theta_{\text{dir}}) \propto \frac{\sin\left(\frac{ka\sin(\theta_{\text{dir}})}{2}\right)}{\frac{ka\sin(\theta_{\text{dir}})}{2}}, \tag{2}$$

where k is the acoustic wave number at the central frequency of the transducer and the size of the transducer. Once again, the angular directivity limits long-distance propagation within a cone whose half-angle depends on the transducer characteristics. Note that in the case of a Pekeris waveguide, we have $\theta_{\text{dir}} = \theta_{\text{grazing}}$ (Fig. 8).

It is interesting to see that the propagation cone in our ultrasonic time-reversal experiments ($\sim 30°$ at -10 dB) is similar to the one measured in underwater acoustics with classical bottom characteristics (typically 15–35° for continental-shelf sediments). This is the reason why time-reversal provides similar results in ultrasonics and in underwater acoustics.

In the free-space visualization, each image of the source and the TRM is weighted according to its attenuation coefficient and the angular directivity (see Fig. 8). Thus, the images further away from the waveguide have a lower contribution to the field.

According to this representation, a time-reversal experiment consists first of transmitting a pulse by all of the sources and second, of time-reversing this field back by the combined TRMs. This leads to a simple algorithm, in the time domain, to compute the acoustic focusing after time reversal:

(1) According to the waveguide characteristics, construct the free-space analog system with the images of the source and the TRM. For a source at coordinates $r_0=(0,y_0)$, the images are at coordinates $r_k=(0,\pm y_0+2kH)$, where k is an integer. For a TRM made of N transducers at $r_i=(L,y_i)$, with $i\in[1,N]$, the TRM images are at $r_{p,i}=(L,\pm y_i+2pH)$, where p is an integer (see Fig. 8).

(2) Compute the Green's functions $G(r_{p,i},t|r_k,0)$ between the sources at r_k and time 0, and the TRMs at $r_{p,i}$ and time t for the forward propagation. Similarly, compute the Green's functions $G(r,t|r_{p,i},0)$ between the TRMs at $r_{p,i}$ and each point $r=(0,y)$, with $y\in[0,H]$ in the plane of the source for the backward propagation. Do not forget the attenuation coefficient of each emitter and the directivity angle of each emitter and each receiver according to their positions.

(3) Compute the time-reversed field at point r using the formula

$$S(r,t)=\sum_k \sum_p \sum_i G(r,t|r_{p,i},0)\otimes G(r_{p,i},T-t|r_k,0) \otimes f(T-t), \tag{3}$$

where $f(t)$ is the transmitted signal and T is such as $G\equiv 0$ for $t>T$. The first sum refers to the source images and the second to the TRM images.

In the case of a uniform sound-speed profile as in the Pekeris waveguide, the acoustic propagation between the sources and the receivers is described by the 3D free-space Green's function, which leads to the simple formula

$$G(r_{p,i},t|r_k,0)\approx R(\theta)\text{ang}^2(\theta)\frac{\delta(t-|r_{p,i}-r_k|/c)}{|r_{p,i}-r_k|} \tag{4}$$

with

$$\theta_{\text{dir}}=\theta_{\text{grazing}}=\theta=\cos^{-1}\left(\frac{|r_{p,i}-r_k|}{L}\right).$$

Note that the angular directivity is squared in Eq. (4) because the field is transmitted and received by transducers with the same characteristics.

If the sound speed is not uniform in the waveguide, then along with each source and TRM there exists a sound-speed profile symmetric with respect to the interfaces. In this case, a ray code must be used to compute the free-space Green's function taking into account acoustic refraction.[21] Off course, time reversal and Eq. (3) remains valid but the new Green's function $G(r_{p,i},t|r_k,0)$ depends dramatically on the sound-speed profile and must be calculated numerically.

The biggest advantage of this algorithm is to work directly in the time domain and to use symmetry properties due to the waveguide geometry to compute the acoustic focusing after time reversal. Thus, in the case of a wideband source, the computational time is greatly reduced compared to the more classical monochromatic-modal formulation of acoustic propagation in a waveguide.

Furthermore, two points are to be underlined:

(i) We have restricted our application of ray theory to a Pekeris waveguide. We have not investigated the classical ray theory problems encountered in a depth-dependent sound-speed profile, such as caustics, for example. Ray theory is a big topic, well-known and available in many references. The aim of this article is not to give a tutorial on this subject but to show that ray tracing is a convenient tool to study time reversal directly in the time domain. Furthermore, even if caustics may dramatically affect the forward propagation between the sources and the TRM by changing the energy distribution in the waveguide, their pres-

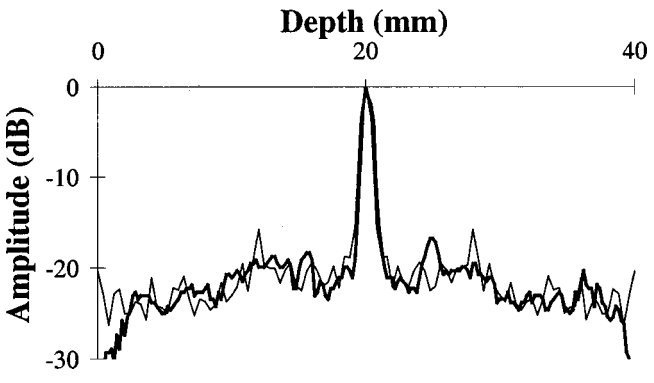

FIG. 9. Directivity pattern of the time-reversed field obtained experimentally (bold line) and numerically (thin line) for a ten-transducer TRM. The TRM spans the whole water depth; $H=40$ mm; source depth$=20$ mm; $L=74$ cm.

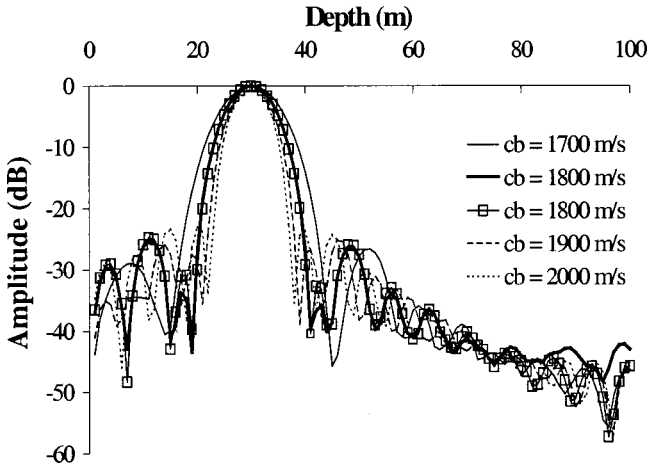

FIG. 10. Directivity pattern of the time-reversed field numerically computed in an underwater waveguide with different bottom velocities *cb*; central frequency$=200$ Hz, -6-dB frequency bandwidth$=50$ Hz, $L=10$ km, $H=100$ m, $\rho_b=2000$ kg/m^3, bottom attenuation$=0.2$ dB/λ, source depth$=30$ m, a 20-transducer TRM. The two $c=1800$ m/s curves correspond to two TRMs whose central position is shifted in depth by 1 wavelength. Since the frequency bandwidth is relatively small, the simulation is based here on normal-mode propagation.

ence does not break time-reversal symmetry and thus, they do not influence the way the time-reversed field focuses back at the source.

(ii) We have described reflection at the water–bottom interface by the reflection coefficient calculated in the case of a monochromatic and plane incident wave. We have not considered the pulse distortion after reflection on this interface which occurs when the reflection coefficient is complex. One way to take care of the pulse distortion is to modify the impulse response (and so the Green's function) as described by Cron *et al.*[22] With a complex reflection coefficient

$$R(\theta)=R_{\text{real}}(\theta)+iR_{\text{imag}}(\theta), \tag{5}$$

the impulse response is no longer defined by $h(t)=R(\theta)\,\delta(t)$, but by the equation

$$h(t)=R_{\text{real}}(\theta)\,\delta(t)-R_{\text{imag}}(\theta)\,\frac{1}{\pi t}. \tag{6}$$

This induces a distortion of the wave, which leads to a spreading of the signal and to a decrease of its amplitude. In order to take care of this wave distortion in our free-space configuration, we use the modified 3D Green's function

$$G(r_{p,i},t|r_k,0)\approx\frac{\text{ang}^2(\theta)}{|r_{p,i}-r_k|}\left(R_{\text{real}}(\theta)\,\delta\left(t-\frac{|r_{p,i}-r_k|}{c}\right)-R_{\text{imag}}(\theta)\,\frac{1}{\pi\left(t-\frac{|r_{p,i}-r_k|}{c}\right)}\right). \tag{7}$$

Figure 9 shows a comparison between an experimental and a numerical directivity pattern obtained after time reversal in an ultrasonic waveguide. The length of the guide is 74 cm, the water depth is 4 cm, and the source is placed at the center of the guide. The TRM is made of ten equally spaced transducers which spread over the whole water depth. The numerical result has been obtained using the algorithm described above and the 3D Green's function as written in Eq. (7). Numerical and experimental results are in good agreement, confirming that a simple model is enough to describe the quality of focusing after time reversal. More particularly, it is obvious that the positions of the source and the TRM in the simulation are not exactly the same as in the experiment. Thus, the good agreement between experimental and numerical results shows that time-reversal focusing is not very sensitive to small errors in the transducer locations.

Indeed, time reversal is known to be a robust process in general and a stable process in the particular case of an acoustic waveguide. Time reversal is robust because it acts as a correlator[11] and is therefore not very sensitive to random noise. The stability of time reversal in a waveguide can be understood through a simple example: suppose the impulse response of the guide is made of ten echoes due to ten reflections on the interfaces. After propagation through the waveguide, the incident field depends on the interference between these ten echoes. It is well-known that the transmitted field is strongly affected by any mismatch of the waveguide characteristics or the receiver location.[23] Suppose now we time-reverse the field by a TRM made of 20 transducers. We are interested now in the time-reversed field in the plane of the source. Because of reciprocity, the impulse response between the TRM and the source is still made of ten echoes. This means that each TRM transducer time-reverses ten echoes and that each of these ten echoes generates ten echoes. For a 20-transducer TRM, the total number of echoes received after time reversal at each point in the plane of the source is then equal to $20\times10\times10=2000$. Once again, all these echoes interfere together and give rise to the spatial and temporal focusing observed in Fig. 2. But, because of the big number of echoes interfering together after time reversal, the time-reversed field appears not to be very sensitive to the phase and to the amplitude of each of them. This means that an approximated knowledge of the transducers location (Fig. 9) or of the bottom characteristics (Fig. 10) does not change time-reversal focusing, whereas it may dramatically affect the incident field. As a consequence, the advantage of the

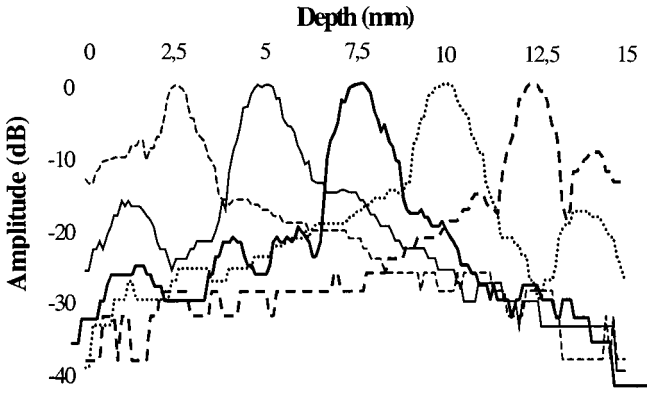

FIG. 11. Experimental directivity pattern of the time-reversed field for five positions of the source y_0 in the waveguide: $y_0=2.5$ mm, $y_0=5$ mm, $y_0=7.5$ mm, $y_0=10$ mm, $y_0=12.5$ mm; $L=74$ cm; $H=1.5$ cm; a 37-transducer TRM.

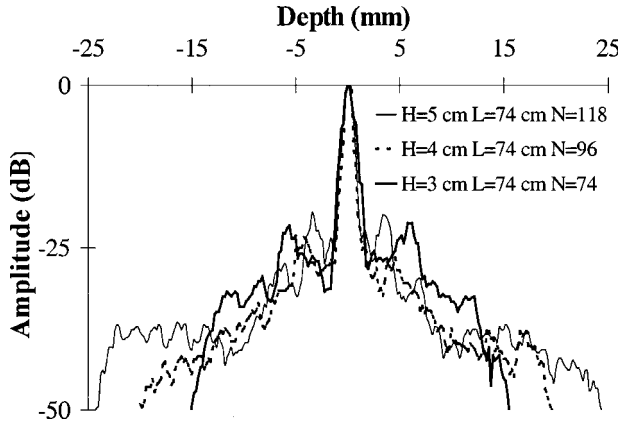

FIG. 12. Experimental directivity pattern of the time-reversed field in three different waveguides. The receiver depth is measured with respect to the source depth y_0: $y_0=15$ mm for $H=30$ mm; $y_0=20$ mm for $H=40$ mm; $y_0=25$ mm for $H=50$ mm. The TRM spans the whole water depth. The width of the focal spot does not change as a function of the waveguide depth.

algorithm described above is that it combines a fast way to compute the time-reversed field and an acceptable accuracy even if the actual environment is roughly simplified.

III. SPATIAL FOCUSING AFTER TIME REVERSAL IN A WAVEGUIDE

The quality of the time-reversal focusing is determined by the characteristic parameters of the TRM-waveguide system. Recall these parameters are the length L, the height (H) of the guide, the wavelength (λ), and the number of transducers (N) of the TRM. In the following, we only work with $L/H \gg 1$ and $H/\lambda \gg 1$.

A. Position of the source

First, we remark that, besides these parameters, the position of the source greatly affects the sidelobe structure. Figure 11 represents five directivity patterns obtained in the same waveguide configuration, which show that the sidelobe levels are dramatically dependent on the depth of the initial source position.

In particular, sidelobes are more important when the source is close to the interfaces. This can be understood easily by the free-space visualization of time reversal in the waveguide. Indeed, the effective source can be considered in free space as the actual source *and* its images. Similarly, time reversal is performed now by the actual TRM *and* its images. This means that the time-reversed field will focus back on each source as seen in Fig. 6. Consequently, if the actual source is close to an interface, the sidelobes of the closest image spill over into the ''real'' waveguide, which explains the results of Fig. 11. For ease of study, we will now always place the source in the middle of the waveguide.

B. Focal spot

The directivity pattern obtained after time reversal in different waveguides is presented in Fig. 12. This figure shows that the focal spot does not depend on the waveguide parameters L or H. According to diffraction laws, the width (Δ) of the focal spot in free space depends on the length of the focusing array (D)

$$\Delta \approx \frac{\lambda L}{D}. \tag{8}$$

In the waveguide, the focal spot is smaller because the reflections of the incident field on the interfaces virtually increase the size of the TRM. The distance D corresponds to the effective aperture of the TRM defined by its images. We have seen in Sec. II that the number of images is limited by two different effects in ultrasonics or in ocean acoustics: in ultrasonics, the field transmitted or received by each transducer is weighted by its angular directivity [Eq. (2)]. Neglecting the reflection coefficient at the steel–water interface, the effective aperture of the TRM is then determined by the product of the angular directivity of the source and the receiver. In our configuration, all the transducers are the same and we call θ_d the half-width directivity angle. Thus, the width of the focal spot is independent of the waveguide and is roughly equal to

$$\Delta \approx \frac{\lambda}{2\tan(\theta_d)}. \tag{9}$$

In an underwater acoustic channel, propagation is also limited inside a cone defined by the critical angle θ_c. However, attenuation in the bottom decreases the contribution of the highest propagating mode as a function of range L. Thus, the width of the focal spot is slowly dependent of L as shown experimentally by Hodgkiss *et al.*[18] This paper roughly defines the width of the focus as the ratio of the water depth to the number of contributing modes if the sound speed is not strongly dependent on depth. In analogy with Eq. (9), this is equivalent to

$$\Delta \approx \frac{\lambda}{2\tan(\theta_m)}, \tag{10}$$

where θ_m is the grazing angle of the highest contributing mode in a waveguide of length L.

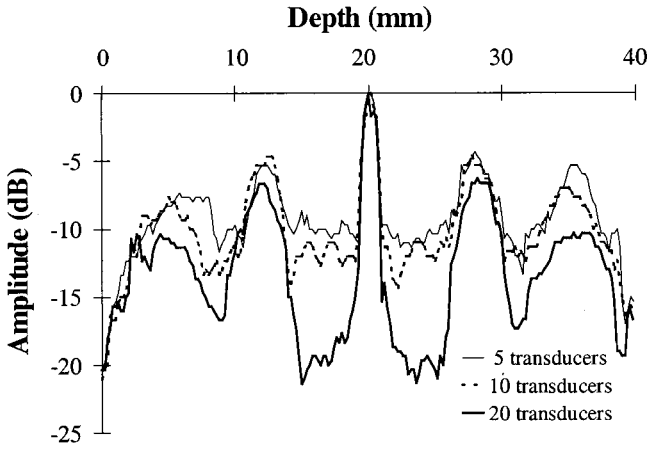

FIG. 13. Directivity pattern of the time-reversed field that puts into evidence sidelobes for small TRMs centered in the waveguide: 5 transducers correspond to a 2.5-mm-large TRM, 10 transducers to a 5-mm-large TRM, and 20 transducers to a 10-mm-large TRM; $H=40$ mm; $L=74$ cm; source depth=20 mm.

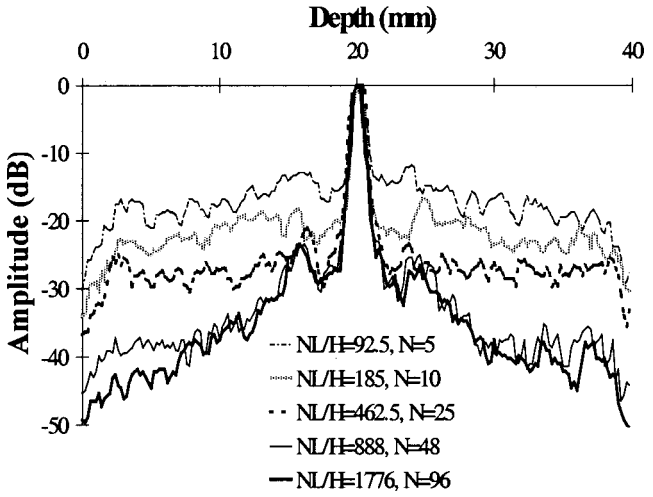

FIG. 14. Experimental directivity pattern of the time-reversed field versus NL/H; the N transducers of the TRM span the whole water depth; $L=74$ cm; $H=40$ mm; source depth=20 mm.

C. Sidelobes

In free space, sidelobes due to spatial aliasing are avoided when the spatial sampling of a horizontal array is greater than or equal to $\lambda/2$. The TRM used in this experiment is a vertical array with λ spacing. This is enough to neglect the sidelobes due to a poor spatial sampling because vertical wavelengths are usually much longer for acoustic waves propagating in a waveguide.[18] However, Fig. 13 represents three directivity patterns obtained after time reversal in a waveguide which clearly show the presence of sidelobes due to spatial aliasing. These sidelobes appear when the TRM becomes small compared to the water depth H because of the new periodicity induced by the guide interfaces. We can visualize then a superarray made up of our small TRMs with spacing H (see Fig. 8). According to diffraction laws, this periodicity generates high sidelobes on each side of the main lobe at distance $k(\lambda L)/H$, where k is an integer. Experimentally, we have $(\lambda L)/H=8$ mm, which corresponds to the position of the sidelobes observed in Fig. 13. In all future measurements, the TRM will adequately span the water column.

We now try to quantitatively understand the dependence of the sidelobes on L, H, and N. The sidelobe amplitude is slowly varying versus water depth, which allows us to define the sidelobe level as its average amplitude around the focal spot. More precisely, we introduced in Sec. I the directivity pattern along the y axis by $d(y)=\max_t\{p_{tr}(y,t)\}$, where $p_{tr}(y,t)$ is the time-reversed beam in the source plane. We now define the sidelobe level by $\langle 20\log_{10}[d(y)]\rangle$ for y varying over five wavelengths on each side of the focal spot. In other words, the sidelobe level is the average envelope expressed in dB around the focal spot. A heuristic study based on the free-space configuration has shown that one of the relevant parameters of the sidelobe study is the number NL/H.[24] We confirm this hypothesis by experimentally and numerically studying the sidelobe level as a function of the three parameters N, L, and H.

Figure 14 represents directivity patterns measured in a waveguide as a function of N. This shows that the sidelobe level decreases as N increases down to a limit reached here when $N\sim 50$, or $NL/H\sim 1000$. Figure 15 represents the sidelobe level measured experimentally and computed numerically as a function of NL/H in different configurations. These results confirm the sidelobe behavior observed experimentally in Fig. 14: the sidelobe level roughly follows an inverse linear decrease as a function of NL/H before reaching a limit for $NL/H\sim 1000$. It is clear that the limit value of the parameter NL/H is not the same for ultrasonic experiments (where it probably depends on the transducer size) and in ocean acoustics (where it surely depends on the bottom property). Thus, the sidelobe level is a very important but very complicated issue. Here are two points that should be theoretically and experimentally investigated in the future:

(i) In our experiments, a saturation of the sidelobe level is clearly observed for $NL/H\sim 1000$ when L/H or N are increased. Increasing N means more transducers

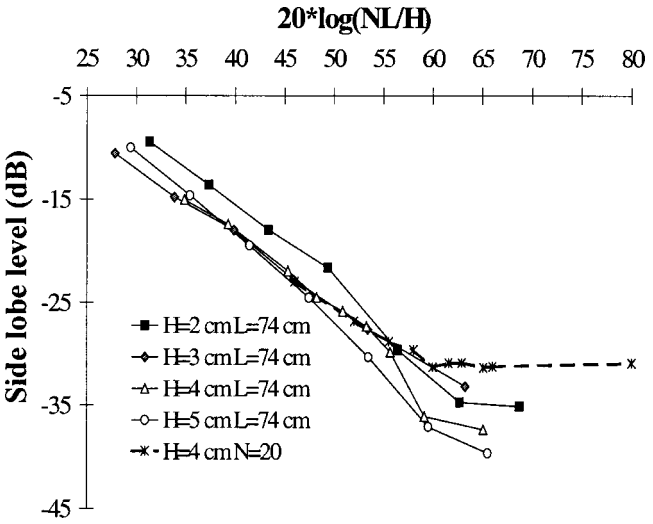

FIG. 15. Logarithmic decrease of the sidelobe level versus NL/H in different waveguides: the first four curves are experimental results as a function of the number of transducers N: the average slope coefficient is equal to -0.92; the dashed line corresponds to numerical results as a function of the waveguide length L and confirms the saturation of the sidelobe level.

and so more spatial information at a given range. Increasing L/H means more reflections on the waveguide interfaces and so more temporal information on each transducer. What is the coupling between spatial and temporal information on the sidelobe level after time reversal?

(ii) What is the effect of the bandwidth of the emitted pulse on the sidelobe level? At first sight, a shorter pulse means a larger bandwidth and leads to lower sidelobes after time reversal.

IV. TEMPORAL COMPRESSION AFTER TIME REVERSAL IN A WAVEGUIDE

We have seen in the Introduction how multipaths were compensated after time reversal in a waveguide [Fig. 3(b)]. Indeed, the time-reversal process enables the realization of an ''optimal'' spatial and temporal filter matched to the waveguide transfer function. This is related to the reciprocity theorem, which states that the positions of a source and receiver can be interchanged without modifying the resulting field. Thus, if the waveguide transfer function is characterized by its impulse response, or equivalently Green's function defined at point r_i and time t by $\tilde{G}(r_i,t|r_s,0)$ from a source at point r_s and time 0, reciprocity means that

$$\tilde{G}(r_i,t|r_s,0)=\tilde{G}(r_s,t|r_i,0). \tag{11}$$

Under this assumption and assuming ideal transducers, the time-reversed field observed at the source location becomes

$$P_{\mathrm{tr}}(r_s=0,t)=\sum_{i=1}^{N}\tilde{G}(r_i,t|r_s=0,0)\otimes\tilde{G}(r_i,T-t|r_s=0,0). \tag{12}$$

Note that the waveguide Green's function $\tilde{G}$ takes into account the reflection on the interfaces and is therefore more complicated than the free-space Green's function G defined in Sec. I.

Each individual contribution i in Eq. (12) is the autocorrelation function of the impulse response between the point r_s and the transducer i at point r_i: it is a symmetrical signal with a maximum at the same time T for each transducer. However, for a given transducer i, the sidelobes of

$$\tilde{G}(r_i,t|r_s=0,0)\otimes\tilde{G}(r_i,T-t|r_s=0,0) \tag{13}$$

are located at different times that depend on the various multipaths between the source and the transducer. When we add a sufficient number of transducers, the sidelobes interfere destructively and all the maxima add constructively at $t=T$. Thus, if the TRM samples the whole water depth, the time-reversed field can be approximated by a Dirac δ-function (Fig. 16). The duration of the time-reversed signal at the initial source is then related only to the transfer function of the transducers, which is actually nonideal.

A. Acoustic transmission using time reversal

The temporal compression observed after time reversal in a waveguide has direct applications to acoustic transmission in underwater acoustics. The issue in underwater acoustic transmission is to send a given signal through a shallow-water environment. If the emitted signal is long, the presence of interfaces leads to the appearance of multiple arrivals, which interfere and damage the quality of the acoustic transmission.

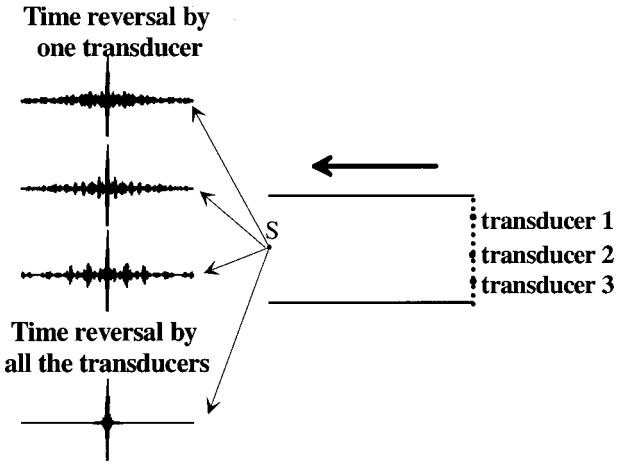

FIG. 16. Temporal compression after time reversal in a waveguide obtained separately for three different transducers and for the whole TRM.

How can a TRM improve acoustic transmissions? Suppose that the goal of a TRM at B is to send a signal $f(t)$ to A through a waveguide (Fig. 1). First, A transmits a short pulse supposed to be a Dirac impulse $\delta(t)$. The TRM at B records the pressure field $h_i(t)$ with $t\in[0,T]$, which is the impulse response of the waveguide between the source and each transducer i of the TRM. After time reversal, we have shown that the time-reversed signal received in A is similar to the emitted Dirac impulse, which means

$$\sum_i h_i(t)\otimes h_i(T-t)=\delta(t). \tag{14}$$

As a matter of fact, if each transducer i of the TRM now transmits the signal $h_i(T-t)\otimes f(t)$, then the signal received at the source A is

$$\sum_i h_i(t)\otimes h_i(T-t)\otimes f(t)=f(t). \tag{15}$$

Following this procedure, Fig. 17 shows the example of the transmission through an ultrasonic waveguide of a train of five pulses. The pulses were separated in time by a time greater than the inverse of the transfer function bandwidth. The quality of the transmission depends dramatically on the number of transducers used on the TRM: the transmission is good for 48 transducers and the signal is unreadable if the time reversal is done with only one transducer. Moreover, we remark that point A is the only place in the waveguide to receive the transmitted information because the time-reversal field is only adapted spatially and temporally at this point. Acoustic transmission using time reversal is then not only accurate but also confidential because the transmitted information will remain obscure to anyone not close to point A.

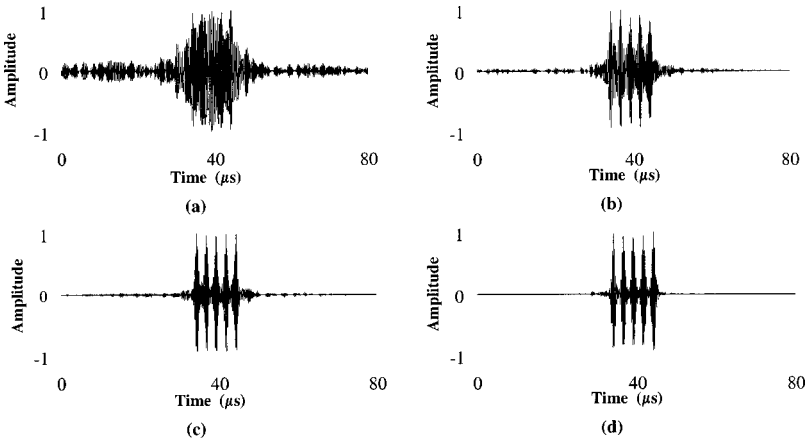

FIG. 17. Acoustic transmission of a train of five pulses using time reversal in a waveguide for a TRM made of (a) 1 transducer, (b) 8 transducers, (c) 16 transducers, and (d) 48 transducers; $L=74$ cm; $H=40$ mm; source depth=20 mm; the TRM spans the whole water depth.

B. Amplification of the signal after time reversal in a waveguide

Another issue of temporal compression is the comparison between the amplitude of the time-reversed signal in the waveguide and in free-space configuration. The presence of interfaces in the guide leads to the generation of multiple echoes, which means that each transducer receives and then retransmits a much bigger energy than in a free-space medium where only one wavefront is expected. After time reversal, all the energy transmitted by the TRM is concentrated on the focal spot. The amplitude of the time-reversed field at the source is then much higher in a waveguide than the amplitude obtained with the same TRM in free space (Fig. 18).

Two points are to be highlighted: both in free space and a waveguide, the amplitude of the time-reversed field increases linearly with the number of transducers on the TRM, because each transducer receives and then retransmits approximately the same energy whatever its position in the waveguide. Generally, this is no longer true in ocean acoustics and, for example, in a strongly down-refracting sound-speed profile where incident energy is refracted to the bottom.[18,25] Next, we see that the shallower the waveguide, the more echoes are received on the TRM and the higher the amplitude of the time-reversed signal at the initial source.

As a matter of fact, the temporal compression may be used to obtain a high-value pressure peak even with a low electrical power input applied to the transducers. Our group is now working on shock wave generators using this principle with a view to medical applications.

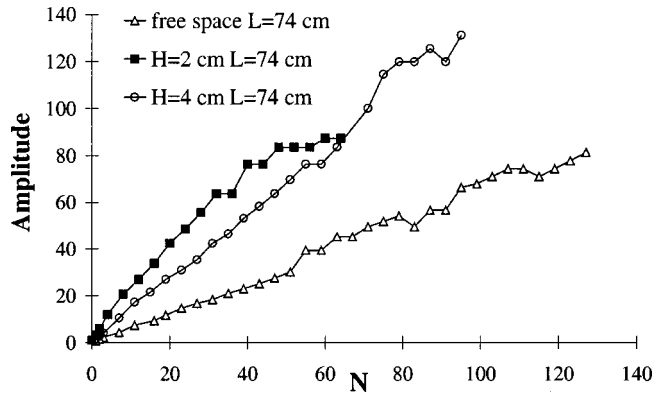

FIG. 18. Comparison of the maximum of the time-reversed signal measured at the source versus N in free space and in two different waveguides.

C. Time reversal in a nonstatic waveguide

We now study the influence of a nonstatic waveguide on the temporal compression observed after time reversal. The waveguide is 74 cm long and 4 cm deep. The 96-transducer TRM spans the whole water depth. Waves at the air–water interface of the guide are generated like waves at the sea surface to create a dynamic interface. The waves propagate from the source toward the TRM and their frequency of excitation is around 15 Hz, which corresponds to a 15-mm wavelength. The root-mean-square height of the waves is on the order of the acoustic wavelength ($\sim$0.5 mm).

First, we remark that the direct wavefront and the wave that reflects only once on the bottom are not affected by this disturbance. Because these echoes are generally the most energetic ones, waves at the sea surface have little effect on time reversal as predicted theoretically by Kuperman *et al.*[17] On the other hand, as soon as the whole time-reversed field is affected by the disturbance, it may have a consequent influence on the time-reversal compression observed at the source. To explore the dynamic effects on time reversal, we select in our time-reversal window only the echoes which have been reflected at least once by the surface of the guide. Then, we perform time reversal in two configurations: an adaptive and a nonadaptive mode. In the adaptive mode, the time-reversed field is transmitted back into the waveguide as fast as allowed by the electronics of the TRM. In the nonadaptive mode, the time-reversed field is delayed before being retransmitted. The time delay is on the order of a few seconds, which is long compared to the dynamic time scale of the surface waves. Figure 19 represents the time-reversed field at the source for 100 shots in the adaptive and the nonadaptive mode.

In the nonadaptive mode, the medium has changed between the reception of the incident field and the transmission of the time-reversed field. The temporal compression at the initial source is then randomly affected by the surface. A similar nonadaptive time-reversal experiment has already been reported in Ref. 18 through an underwater acoustic channel where the disturbances were probably due to internal waves evolving on a few minutes' time scale.

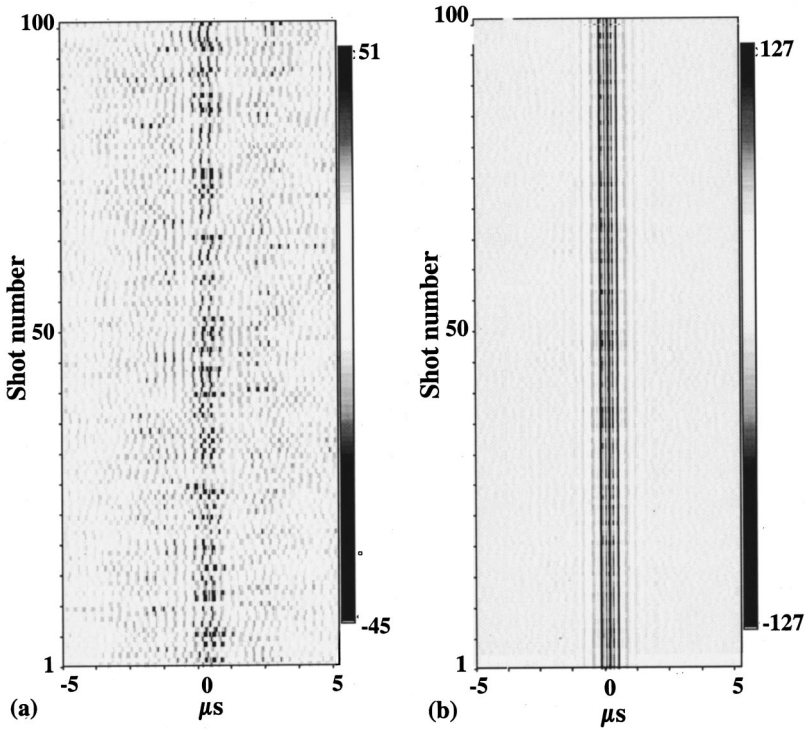

FIG. 19. Representation of 100 successive time-reversed signals measured at the source in an unstationary waveguide: (a) in the nonadaptive mode, (b) in the adaptive mode. The x axis corresponds to the time and the y axis to the shot number. The gray scale corresponds to the amplitude of the time-reversed signal. $L=74$ cm; $H=40$ mm; a 96-transducer TRM.

In the adaptive mode, the time-reversal process and the acoustic propagation is short enough ($\sim$2 ms) to consider the nonstatic surface as frozen during this time interval. In this case, the surface waves act as a rough static interface and the temporal compression after time reversal is similar to the one observed in a plane waveguide. In the ocean, acoustic propagation in shallow water lasts mostly between 1 and 20 s. Compared to the internal dynamic time scale of the ocean (around a few minutes), it should be possible to perform a good and stable time-reversal compression with a TRM working in the adaptive mode.

Finally, we quantify the effect of the nonstatic surface by a statistical study of the time-reversed amplitude at the source in the adaptive and nonadaptive mode (Fig. 20). As expected, we observe that the average amplitude in the nonadaptive mode is four times weaker than in the adaptive mode, which is itself close to the time-reversed amplitude obtained in a plane and static waveguide.

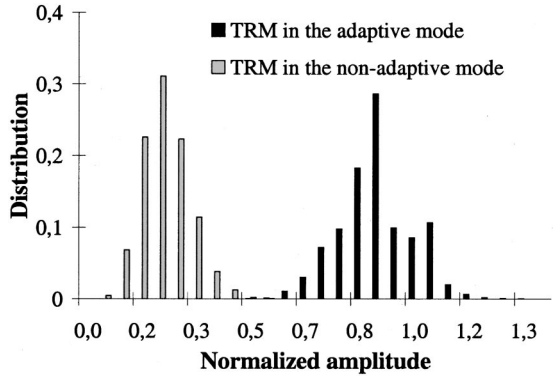

FIG. 20. Distribution of the amplitude maxima of 5000 time-reversed signals measured at the source in an unstationary waveguide. Amplitude 1 corresponds to the maximum of the time-reversed signal at the source in a static waveguide; $L=74$ cm; $H=40$ mm; a 96-transducer TRM.

V. CONCLUSION

We have presented in this paper experimental and numerical results on time-reversal properties in an ultrasonic waveguide. As long as the basic differences between ultrasonics and ocean acoustics are understood, some of these results are applicable to an underwater acoustic channel. We have shown in particular that the spatial sidelobe level around the focal spot depends on NL/H, where L and H are the length and the height of the guide and N the number of transducers of the TRM. On the other hand, the temporal compression observed after time reversal may lead to applications to acoustic transmission in ocean acoustics as well as high-intensity focusing in the medical field. Following some recent works in a wedge waveguide,[26] we plan to experimentally and numerically study time-reversal focusing in range-dependent waveguides in the future.

ACKNOWLEDGMENTS

The authors would like to thank Julien De Rosny for his useful contribution to the experiments and James H. Rose, Geoffrey Edelmann, and the referees for their wise comments on the manuscript.

[1] D. Cassereau and M. Fink, ''Time-reversal of ultrasonic fields. III. Theory of the closed time-reversal cavity,'' IEEE Trans. Ultrason. Ferroelectr. Freq. Control **39**, 579–592 (1992).
[2] D. Cassereau and M. Fink, ''Focusing with plane time-reversal mirrors: An efficient alternative to closed cavities,'' J. Acoust. Soc. Am. **94**, 2373–2386 (1993).
[3] M. Fink, C. Prada, F. Wu, and D. Cassereau, ''Self-focusing in inhomogeneous media with time-reversal acoustic mirrors,'' Proc. IEEE Ultrason. Symp. (2), 681–686 (1989).
[4] M. Fink, ''Time-reversal of ultrasonics fields. I. Basic principles,'' IEEE Trans. Ultrason. Ferroelectr. Freq. Control **39**, 555–566 (1992).
[5] M. Fink, ''Time-reversal in acoustics,'' Contemp. Phys. **37**(2), 95–109 (1996).

[6] M. Fink, ''Time-reversed acoustics,'' Phys. Today **50**(3), 34–40 (1997).
[7] A. Derode, P. Roux, and M. Fink, ''Robust acoustic time-reversal with high-order multiple scattering,'' Phys. Rev. Lett. **75**, 4206–4209 (1995).
[8] C. Draeger and M. Fink, ''One-channel time-reversal of elastic waves in a chaotic 2D silicon cavity,'' Phys. Rev. Lett. **79**, 407–410 (1997).
[9] P. Roux, B. Roman, and M. Fink, ''Time-reversal in an ultrasonic waveguide,'' Appl. Phys. Lett. **70**(14), 1811–1813 (1997).
[10] A. Parvulescu and C. S. Clay, ''Reproducibility of signal transmissions in the ocean,'' Radio Electron. Eng. **29**, 223–229 (1965).
[11] A. Parvulescu, ''Matched-signal (Mess) processing by the ocean,'' J. Acoust. Soc. Am. **98**, 943–960 (1995).
[12] D. R. Jackson and D. R. Dowling, ''Phase-conjugation in underwater acoustics,'' J. Acoust. Soc. Am. **89**, 171–181 (1991).
[13] D. R. Dowling and D. R. Jackson, ''Narrow-band performance of phase-conjugate arrays in dynamic random media,'' J. Acoust. Soc. Am. **91**, 3257–3277 (1992).
[14] D. R. Dowling, ''Phase-conjugate array focusing in a moving medium,'' J. Acoust. Soc. Am. **94**, 1716–1718 (1993).
[15] D. R. Dowling, ''Acoustic pulse compression using passive phase-conjugate processing,'' J. Acoust. Soc. Am. **95**, 1450–1458 (1994).
[16] C. Feuillade and C. S. Clay, ''Source imaging and sidelobe suppression using time-domain techniques in a shallow-water waveguide,'' J. Acoust. Soc. Am. **92**, 2165–2172 (1992).
[17] W. A. Kuperman, W. S. Hodgkiss, H. C. Song, T. Akal, C. Ferla, and D. R. Jackson, ''Phase conjugation in the ocean: Experimental demonstration of an acoustic time-reversal mirror,'' J. Acoust. Soc. Am. **103**, 25–40 (1998).
[18] W. S. Hodgkiss, H. C. Song, W. A. Kuperman, T. Akal, C. Ferla, and D. R. Jackson, ''A long-range and variable focus phase conjugation experiment in shallow water,'' J. Acoust. Soc. Am. **105**, 1597–1604 (1998).
[19] C. L. Pekeris, ''Theory of propagation of explosive sound in shallow water,'' Mem.-Geol. Soc. Am. **27** (1948).
[20] L. M. Brekhovskikh and Y. P. Lysanov, *Fundamental of Ocean Acoustics*, 2nd ed. (Springer, New York, 1990).
[21] F. B. Jensen, W. A. Kuperman, M. B. Porter, and H. Schmidt, *Computational Ocean Acoustics* (Springer, New York, 1994).
[22] B. F. Cron and A. H. Nuttal, ''Phase distortion of a pulsed caused by bottom reflection,'' J. Acoust. Soc. Am. **37**, 486–492 (1965).
[23] A. B. Baggeroer, W. A. Kuperman, and H. Schmidt, ''Matched field processing: Source localization in correlated noise as an optimum parameter estimation problem,'' J. Acoust. Soc. Am. **83**, 571–587 (1988).
[24] P. Roux, ''The acoustic time reversal mirrors: Application to the focalization in a waveguide and to the characterization of hydrodynamic flows,'' Thesis (in French), Paris VI University, 1997.
[25] H. C. Song, W. A. Kuperman, and W. S. Hodgkiss, ''A time-reversal mirror with variable range focusing,'' J. Acoust. Soc. Am. **103**, 3234–3240 (1998).
[26] C. Feuillade and C. S. Clay, ''Broadband source imaging in a shallow water wedge by an array of receivers,'' J. Acoust. Soc. Am. **96**, 501–504 (1994).